Analysis of NO_X Formation in an Axially Staged Combustion System at Elevated Pressure Conditions

Chockalingam Prathap
Flavio C. C. Galeazzo
Plamen Kasabov
Peter Habisreuther
Nikolaos Zarzalis

Division of Combustion Technology,
Engler-Bunte-Institute,
Karlsruhe Institute of Technology,
Engler-Bunte-Ring 1,
76131 Karlsruhe, Germany

Christian Beck
Werner Krebs
Bernhard Wegner

SIEMENS AG,
Mellinghoferstr. 55,
45473 Mülheim an der Ruhr, Germany

The objective of this investigation was to study the effect of axially staged injection of methane in the vitiated air cross flow in a two stage combustion chamber on the formation of NO_X for different momentum flux ratios. The primary cylindrical combustor equipped with a low swirl air blast nozzle operating with Jet-A liquid fuel generates vitiated air in the temperature range of 1473–1673 K at pressures of 5–8 bars. A methane injector was flush mounted to the inner surface of the secondary combustor at an angle of 30 deg. Oil cooled movable and static gas probes were used to collect the gas samples. The mole fractions of NO, NO_2, CO, CO_2, and O_2 in the collected exhaust gas samples were measured using gas analyzers. For all the investigated operating conditions, the change in the mole fraction of NO_X due to the injection of methane (ΔNO_X) corrected to 15% O_2 and measured in dry mode was less than 15 ppm. The mole fraction of ΔNO_X increased with an increase in mass flow rate of methane and it was not affected by a change in the momentum flux ratio. The penetration depth of the methane jet was estimated from the profiles of mole fraction of O_2 obtained from the samples collected using the movable gas probe. For the investigated momentum flux ratios, the penetration depth observed was 15 mm at 5 bars and 5 mm at 6.5 and 8 bars. The results obtained from the simulations of the secondary combustor using a RANS turbulence model were also presented. Reaction modeling of the jet flame present in a vitiated air cross flow posed a significant challenge as it was embedded in a high turbulent flow and burns in partial premixed mode. The applicability of two different reaction models has been investigated. The first approach employed a combination of the eddy dissipation and the finite rate chemistry models to determine the reaction rate, while the presumed JPDF model was used in the further investigations. Predictions were in closer agreement to the measurements while employing the presumed JPDF model. This model was also able to predict some key features of the flow such as the change of penetration depth with the pressure.
[DOI: 10.1115/1.4004720]

Introduction

Lifted turbulent non-premixed flames are found in many practical applications like burners in boilers, direct fuel injection gasoline engines, and also gas turbines. Owing to their importance, they have received a large amount of attention in the last 50 years. The prime objective of all the studies is to understand the conditions under which the lifted flame stabilizes and also their associated causes [1–4]. The advantages of such flames are that they produce significantly lower NO_X emissions compared to the burner attached turbulent non-premixed flames. A detailed review on stabilization and blow out mechanisms of turbulent jet flames was given by Pitts [1]. Peters [2] quoted that theory based on partial premixing predicts the lift-off height of a turbulent jet flame which matches closely with the experimental data. Lyons [3] in his review mentioned that theories based on partial premixing and edge flames are the foremost theories considered for the determination of lift-off height of the diffusion flame. In a recent review, Lawn [4] had discussed the effect of co-flowing fluid on the stabilization of turbulent jet flames. The abovementioned reviews mainly discussed the stabilization mechanisms and also the determination or estimation of lift-off height of the turbulent jet flames with or without co-flow studied at atmospheric condition.

Kalghatgi [5–7] measured the lift-off height of turbulent hydrogen, propane, ethylene, and methane flames for a wide range of nozzle diameters and jet velocities. He mentioned that lift-off height varies linearly with the jet velocity, and it was nearly independent of the burner diameter. Han and Mungal [8] experimentally investigated the stabilization regime of two turbulent lifted deflected ethylene jet flames injected at an angle of 45 deg into a cross flow against the flow direction. They varied the cross flow speeds from 1.8 to 3 m/s. They used CH planar laser-induced fluorescence and particle image velocimetry to obtain the flame base location and the velocity field. They mentioned that their observations were in line with the concept that the velocity at the flame base is proportional to the stoichiometric velocity.

Johnson et al. [9] utilized a novel low swirl injector in a confined chamber to produce a lifted flame with ultra low NO_X emissions for gas turbine conditions using methane-air premixed mixtures. They also calculated the turbulent flame speed from their experiments. Littlejohn and Chen [10] extended the work of Johnson et al. [9] and studied the characteristics of low swirl burners for premixed diluted and undiluted hydrocarbon and hydrogen fuels. Fokaides et al. [11] investigated lifted flame developed by a low swirl air blast nozzle operating with non-premixed Jet-A-air mixture in a confined chamber at both atmospheric and high pressure conditions. They mentioned that the lean blow out limit was significantly increased with a lifted flame compared to an attached flame leading to low NO_X emissions. Kasabov and Zarzalis [12] had investigated experimentally the characteristics of low swirl air blast nozzles in a confined chamber operating with non

Contributed by the international Gas Turbine Institute (IGTI) of ASME for publication in the Journal of Engineering for Gas Turbines and Power. Manuscript received April, 29, 2011; final manuscript received July 13, 2011; published online January 4, 2012. Editor: Dilip R. Ballal.

premixed Jet-A-air mixtures at elevated pressures. They reported NO_X emissions below 20 ppm corrected to 15% O_2 for all the investigated operating conditions. Cabra et al. [13,14] investigated both numerically and experimentally the lift-off height of H_2/N_2 and methane turbulent jet flames in the presence of a hot vitiated co-flow of air at atmospheric pressure. They commented that turbulent premixed flame propagation by small scale recirculation and mixing of hot products into reactants and subsequent rapid ignition of the mixture was responsible for the stabilization of the turbulent jet flame at the lift-off height. Hayashi and Himada [15] proposed a two-stage combustor concept for achieving stable combustion with ultra-low NO_X emissions for a wide range of operating conditions at atmospheric pressure. In their two-stage premixed combustor, the first stage was utilized to burn a lean premixed methane-air mixture of a fixed equivalence ratio, and in the second stage, they injected a lean premixed mixture of methane-air into the hot burned gas from the first stage. They fixed the mass flow rates of air in both the stages and also maintained a constant flow rate of fuel in the first-stage. Then, they varied only the secondary fuel flow rate to cover the range of fuel-air ratios utilized in a gas turbine. With their new concept, they achieved stable combustion with ultra-low NO_X emissions over a wide range of overall equivalence ratios for an inlet air temperature at 573 K, which was wider than that of single stage combustion system. Hayashi et al. [16] extended their previous work and investigated the NO_X emissions of combustion of kerosene fuel in the two-stage combustor at 8 bars and 600 K. Adachi et al. [17] developed a three stage combustor operating at atmospheric pressure. They injected the secondary premixed mixture either methane-air or biomass gas-air into the cross flow of hot exhaust gases from the primary stage combustor. They also mentioned that the complete combustion of the secondary and tertiary staged injected mixtures were possible if the temperature of the hot exhaust gases from the primary stage is greater than 1500 K. No literature data, i.e., neither experimental nor numerical, are available on the characteristics such as penetration depth and lift-off height of a secondary jet flame anchored in a cross flow stream of hot air or hot vitiated air.

In the present work, NO_X emissions from a two stage cylindrical combustor at elevated pressures were investigated. The main objective of this work was to analyze the effect of the axially staged injection of methane on the global NO_X emissions of a two stage combustion system for different combustion chamber pressures (absolute) and momentum flux ratios. The reason for the angled injection of methane into the vitiated air cross flow was to prevent the impingement of methane on the wall of the secondary combustor. An attempt was made to measure the penetration depth of the secondary jet flame using a movable single port gas suction probe. The NO_X emissions generated due to the addition of methane in the secondary stage was investigated for the following operating conditions:

- temperature of vitiated air: 1473–1673 K
- pressure of vitiated air: 5–8 bars (absolute)
- momentum flux ratio of the methane jet to the vitiated air: 5–375

A numerical study was performed in order to evaluate the predictability of the lift-off height using CFD simulations. Furthermore, the measurements have shown that the flow and mixing fields change when the pressure is increased, which make it impossible to extrapolate the results from low to high pressure systems. The ability of two different reaction models (a combination of the eddy dissipation and the finite rate chemistry models and the presumed JPDF model) in predicting the difference in the jet penetration depth due to the pressure variation was investigated.

Experimental Facility and Procedure

Figure 1 shows the layout of the experimental setup used in the present work. It has two stages, and the flow direction is from top to bottom. The first stage comprised a pulsation damper and a primary combustor. The pulsation damper was a tubular stainless steel chamber with an inner diameter of 150 mm and a length of 150 mm. The pulsation damper was used to ensure uniform flow rate of combustion air to the air blast nozzle by eliminating the fluctuations in the incoming compressed air. The low swirl air blast nozzle was flush mounted at one of the flanges of the pulsation damper in the downstream flow direction. The design details of the air blast nozzle were given elsewhere [11,12]. The air blast nozzle will stabilize lifted flames burning at lean mixture conditions to generate vitiated air with low NO_X emissions for all the investigated operating conditions. To stabilize a lifted flame successfully in the present air blast nozzles, the pressure drop across the nozzle has to be close to 3% [11,12]. For the present test conditions, two different nozzles with effective areas of 319 mm^2 and 212 mm^2 developed by Kasabov and Zarzalis [12] were utilized. The liquid fuel (Jet-A) from a high pressure pipe was injected into the axis of the air blast nozzle using a hollow cone atomizer. The compressors in our research laboratory can supply a maximum air mass flow rate of 125 g/s at a pressure of 40 bars.

The pulsation damper with the air blast nozzle was mounted on the primary combustor. The primary combustor was a tubular ceramic pipe with an inner diameter of 100 mm, and it was secured in a water-cooled stainless steel housing. The ceramic pipe was used as a combustor in order to minimize the heat losses and to maintain an almost adiabatic condition in the combustor. The vitiated air generated by the primary stage combustion exhibits swirl effects and flow field irregularities. It was very important to eliminate these flow field irregularities from the vitiated air before it reached the secondary combustor. For eliminating the flow field irregularities, a cylindrically shaped porous foam monolith made of aluminum oxide was used in the downstream end of the primary combustor as shown in Fig. 1. It enhanced the homogeneity in the distribution of species, velocity, and temperature in the vitiated air.

Then the secondary combustor followed the primary combustor as shown in Fig. 1. The secondary combustor was also a ceramic pipe, and it was also secured in a water-cooled stainless steel housing. The inner diameter of the secondary combustor was 50 mm in order to achieve the desired flow velocity with the available mass flow rates of combustion air. The secondary combustor has ports for a methane injector, thermocouples, and a gas sampling probe. The methane injector was an oil cooled tubular burner. It was flush mounted to the inner surface of the secondary combustor at an angle of 30 deg to the axis. An oil cooled movable single port gas probe was mounted 721 mm downstream of the air blast nozzle as shown in Fig. 1. It was used for collecting gas samples at various radial positions in the secondary combustor for gas analysis. The gas probes and methane injector were oil cooled to prevent them from damaging as they were exposed to hot exhaust gases. The gas probes were maintained at 425 K in order to quench the chemical reaction in the gas samples and also to prevent the condensation of water vapor and unburned hydrocarbon vapors. The vitiated air temperature was measured using the thermocouples mounted in the secondary combustor, which were placed downstream of the porous structure as shown in Fig. 1. The measured vitiated air temperature was used to control the air-fuel ratio of the primary stage combustion process in turn to attain the desired vitiated air temperature.

A buffer chamber with a water cooled static mixer followed the secondary combustor. The injection of methane from one side of the secondary combustor into the vitiated air leads to a mixture with a high degree of unmixedness of unutilized vitiated air and secondary stage combustion products at the end of the secondary combustor. Hence a water cooled static mixer was used to enhance the mixing of the unutilized vitiated air and the secondary stage combustion products. A static oil cooled multi port gas probe was mounted in the bottom flange of the buffer chamber, 947 mm downstream of the air blast nozzle. An exhaust gas cooling system followed the buffer chamber. A manually operated

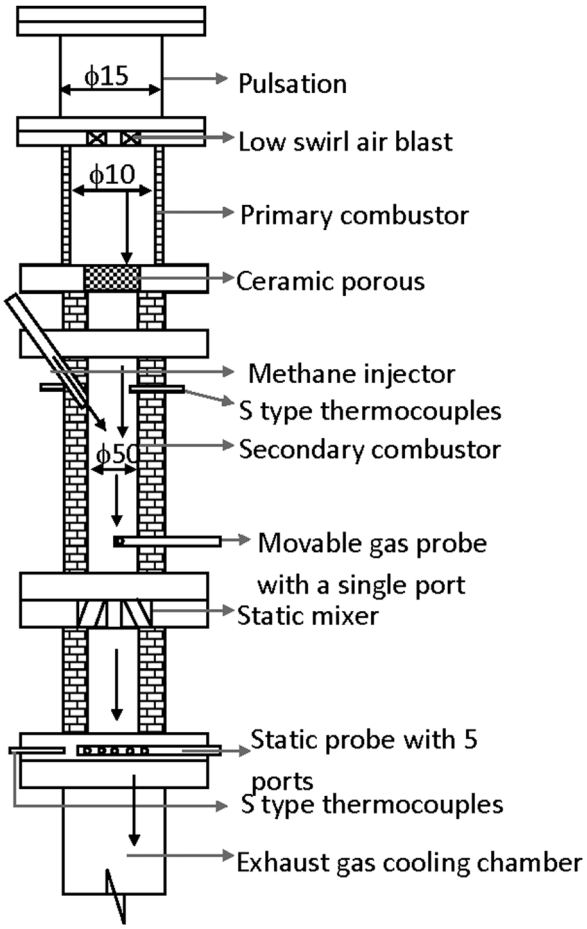

Fig. 1 Schematic layout of the experimental facility

gate valve was mounted after the exhaust gas cooling system, which was used to control and to maintain the required pressure in the combustor rig.

Operation Procedure

The combustion air was preheated in a 24 kW electrical preheater, and it was supplied to the pulsation damper. The mass flow rate of combustion air was measured using an orifice plate mounted upstream of air preheater. The temperature of the preheated combustion air was measured using a K-type thermocouple. The pressure drop across the air blast nozzle was measured using a differential pressure transducer. The mass flow rate of Jet-A fuel injected into the primary combustor was measured using a digital mass flow meter. A pilot hydrogen flame burner was used for ignition in the primary stage. Then, the mass flow rates of air and fuel in the primary combustor were adjusted to generate vitiated air at the required pressure and temperature. The temperature of vitiated air in the secondary combustor was monitored using four different S-type thermocouples located at different radial and circumferential positions upstream of the methane injector as shown in Fig. 1. The pressure in the secondary combustor was measured using a static, absolute pressure transducer. Electrically heated high pressure hoses maintained at 425 K were used to transport the gas samples from the gas probes to a dryer and then to the exhaust gas analyzers. The mole fractions of O_2, NO, NO_2, CO, and CO_2 were measured from the dried gas samples. For the measurement of unburned hydrocarbons in the gas samples, separate electrically heated hoses were used to carry the wet gas samples from the gas probes to the unburned hydrocarbon analyzer. The entire measurement system was monitored using LabVIEW® and all the measurement data were logged into a computer at an interval of every 500 milliseconds.

First, the primary combustor was operated and the vitiated air was generated according to the required operating condition. Then, the samples of vitiated air were collected using a static multiport gas probe, and its composition was analyzed. Then, the movable probe was traversed into the secondary combustor until the desired radial position and the gas samples from that position were collected and analyzed. Similarly, the composition of the gas in the secondary combustor was measured at five different locations by traversing the movable single port gas probe. After the successful characterization of the vitiated air, the methane was injected and the gas samples were collected and analyzed. The same procedure was repeated for all the investigated operating conditions.

Results and Discussion

The experiments were conducted as follows. First, the properties such as temperature and composition of vitiated air were measured without the injection of methane in the secondary stage. Then, the methane was injected in the secondary stage, and the mole fractions of the NO_X, O_2, CO, CO_2, and Unburned Hydro Carbons (UHC) were measured. Finally, the difference between them was deduced in order to quantify the contribution of secondary injection on the overall NO_X emission of the present two stage combustion chamber.

Analysis of Vitiated Air

The measurement of the properties of the vitiated air was very important for the accurate analysis of the effect of the secondary methane injection. It is important to ensure a uniform flow field of vitiated air in the secondary combustor with a homogeneous composition in order to minimize the possible uncertainties arising in the measurements due to flow field irregularities. The homogeneity in the composition of the vitiated air was verified by the comparison of:

- the air to fuel ratio based on mass calculated from the measured mass flow rates of both fuel (Jet-A) and air. It will be referred as AFR-performance.
- the air to fuel ratio based on mass calculated from the composition of the vitiated air measured from gas analyzers, and it will be called AFR gas analysis.

Figure 2 shows the variation of AFR gas analysis with AFR performance for vitiated air without methane injection. The reference line represents a perfect match between both the AFR gas analysis and AFR performance. AFR gas analysis was calculated from the analysis of samples of vitiated air collected using the static multiport gas probe. For most of the investigated operating conditions, the comparison between the AFR gas analysis and AFR performance is excellent. The maximum deviation between the AFR performance and AFR gas analysis obtained was 9.5%. This indicates that the vitiated air generated by the primary stage combustor has homogenous composition for all the investigated operating conditions. This was also verified from the comparison of the mole fraction of O_2 measured from the analysis of gas samples collected using a movable single port gas probe at five different radial locations in the secondary combustor, and it is shown in Fig. 5. The values of mole fraction of O_2 measured from all the five radial locations are nearly the same indicating the homogeneity in the composition of vitiated air in the secondary combustor.

Mole Fraction of NO_X in Vitiated Air

Figure 3 shows the variation of mole fraction of NO_X corrected to 15% O_2 with the adiabatic flame temperature of the vitiated air for different pressures in the combustion chamber in the absence of secondary stage methane injection. The mole fraction of NO_X

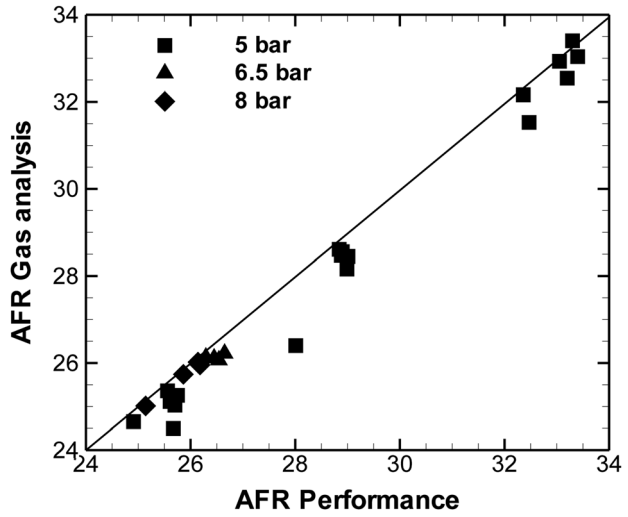

Fig. 2 AFR-gas analysis versus AFR performance of vitiated air without methane injection for vitiated air temperature (T_{va}) = 1473–1673 k at 5–8 bars

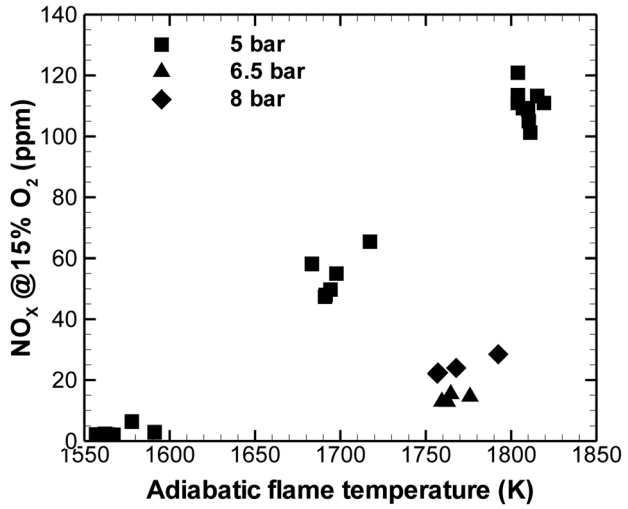

Fig. 3 Mole fraction of NO_X at 15% o_2 (ppm) versus adiabatic flame temperature (K) of the vitiated air generated using two different air blast nozzles for different equivalence ratios and vitiated air temperatures (T_{va}) at different pressures

in the vitiated air was measured from the analysis of the gas samples of vitiated air collected using the static multi port gas probe. It is important to mention here that the NO_X emissions were plotted as a function of the adiabatic flame temperature calculated for each operating condition rather than the measured values of the vitiated air temperature. The reason was that the desired value of vitiated air temperature was achieved by varying the equivalence ratio in the primary combustor to compensate for the small changes in the inlet temperature of combustion air, which leads to a simultaneous change in the adiabatic flame temperature and NO_X formation. It is difficult to show the aforementioned variations when the NO_X is plotted as a function of vitiated air temperature.

Figure 3 clearly depicts that as the adiabatic flame temperature increased, the NO_X emissions also increased significantly because of an increase in the formation rate of thermal NO_X. A maximum value of 120 ppm of NO_X corrected to 15% O_2 was measured in the vitiated air at 5 bars and 1673 K. It is higher than the targeted value of 10–20 ppm. The reason for the increased NO_X emissions for the above mentioned operating conditions could be a difference in the flame configuration in the primary combustion chamber. By design, the flame generated by the applied air blast nozzles should be a lifted partially premixed flame [11,12]. In the liftoff zone, the liquid fuel pre-vaporizes and mixes with the surrounding air before approaching the flame front. The flame stabilized at the end of the liftoff height is a lean partially premixed flame leading to a low level of NO_X emissions. As mentioned earlier the pressure drop across the air blast nozzles has to be approximately 3% to anchor a lifted lean partially premixed flame [12]. Table 1 shows the values of the measured pressure drop across the applied air blast nozzles for all the investigated operating conditions. The table indicates that the pressure drop for the experiments performed at 5 bars is in the range of 1.2–2.96%. In the given pressure drop range at 5 bars (a) the smaller values of pressure drop correspond to experiments with an adiabatic flame temperature of 1650–1850 K, which possibly indicates that the established flame for these conditions was not a lifted partially premixed flame. Instead it could be an attached flame which burns in the diffusion mode with higher flame temperatures resulting in high level of NO_X emissions, and (b) the higher values of pressure drop correspond to experiments with adiabatic flame temperature lower than 1600 K, which indicate higher chances of a lifted partially premixed flame, leading to a lower level of NO_X emissions. Also for the above mentioned operating conditions, the production rate of thermal NO_X is also lower as the adiabatic temperature is lower, resulting in further lower levels of NO_X emission. It is important to mention here that even for these operating conditions with slightly higher values of NO_X in the vitiated air, the additional NO_X generated by the secondary injection was measured accurately.

Table 1 Effective area of the air blast nozzles and pressure drop across it for different pressures

Effective area of air blast nozzle (mm^2)	Pressure (bar)	Pressure drop across the air blast nozzle
319	5	1.2–2.96%
212	6.5	3.33–3.67%
212	8	3.15–3.42%

Figure 3 also shows that for a given range of adiabatic flame temperature (1750–1825 K), if the combustion chamber pressure is increased from 5 to 6.5 or 8 bars, the NO_X emissions decreased drastically. These measurements had been performed with a nozzle with smaller effective area of 219 mm^2 and the pressure drop across it has been shown in Table 1. The pressure drop across this air blast nozzle used for high pressures is always greater than 3%, which is sufficient for stabilizing a lifted partially premixed flame [11,12]. The values of mole fraction of NO_X corrected to 15% O_2 measured for these operating conditions were close to 20 ppm. This clearly indicates that if the pressure drop across the applied air blast nozzles was close to 3%, it produced a lifted partially premixed flame leading to very low NO_X emissions even for high operating temperatures and pressures.

ΔNO_X Emissions for Different Momentum Flux Ratios

Figure 4 shows the variation of change in the mole fraction of NO_X (ΔNO_X) corrected to 15% O_2 with the change in the adiabatic flame temperature (ΔT) due to the methane injection for the following operating parameters:

- inner diameter of the methane injector = 0.8 mm
- vitiated air temperature, $T_{VA} = 1673$ K
- pressure, p = 5, 6.5 and 8 bars
- momentum flux ratio = 5–375
- velocity of vitiated air in the secondary combustor = 40 m/s

In the same figure, the mole fraction of ΔNO_X obtained for a ΔT of 63 K and a momentum flux ratio of 202 was also shown as

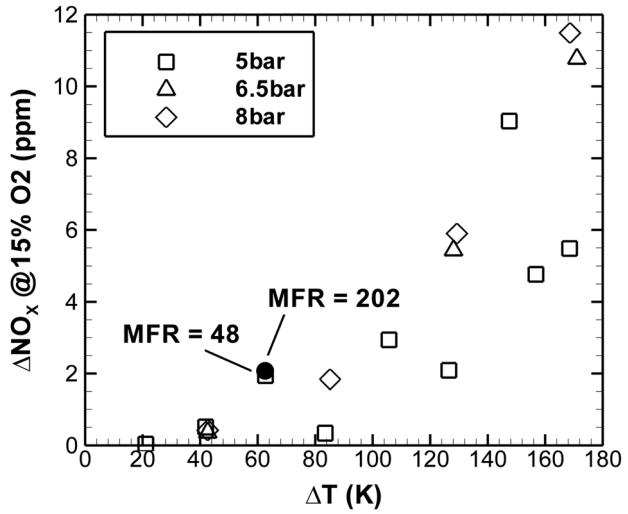

Fig. 4 Mole fraction of ΔNO_x (ppm) versus ΔT (K) for the methane injector with an inner diameter of 0.8 mm, $T_{va} = 1673$ K, pressure = 5, 6.5 and 8 bars. Momentum flux ratio for 5 bars = 5–365 and for 6.5 and 8 bars = 22–375.

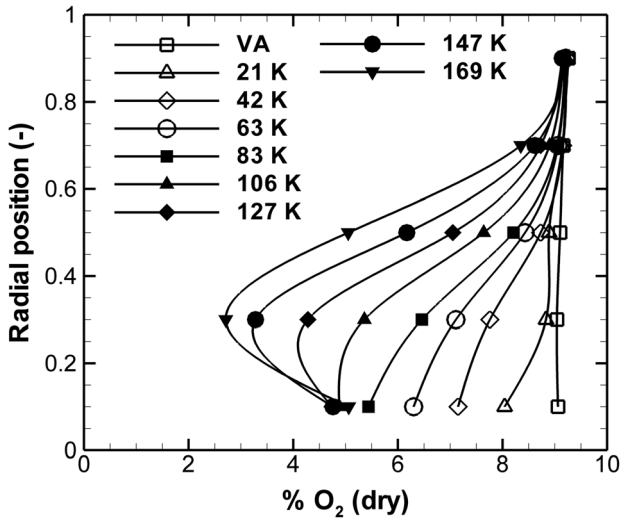

Fig. 5 Mole fraction of O_2 (dry) measured at different radial positions in the secondary combustor for $T_{va} = 1673$ K at 5 bars. The line legend titles represent ΔT in K. VA represents vitiated air, i.e., measurement without methane injection.

a solid circle. The increase in the mass flow rate of methane leads to a simultaneous increase in both the ΔT and momentum flux ratio respectively. One interesting observation is that for all the studied conditions mentioned above, the mole fraction of ΔNO_X (ppm) corrected to 15% O_2 is always close to 10 ppm. Figure 4 shows that if the ΔT is lower than 100 K, the mole fraction of ΔNO_X at 15% O_2 is close to zero. With further increases in ΔT above 100 K, the mole fraction of ΔNO_X at 15% O_2 also increased due to the increase in the production of thermal NO_X. Figure 4 indicates that the mole fraction of ΔNO_X is not influenced by an increase in the momentum flux ratio from 48 to 202 for a fixed value of $\Delta T = 63$ K. The above discussion clearly states that the mole fraction of ΔNO_X is sensitive to ΔT, and it is not influenced by the momentum flux ratio. But the design was that with an increase in the momentum flux ratio, the liftoff height and the penetration depth of the methane jet should increase, leading to a lean premixed flame and resulting in a very small change in the mole fraction of ΔNO_X even with an appreciable increase in the ΔT. The increase in the mole fraction of ΔNO_X with an increase in ΔT indicates the higher chances of a diffusion mode of secondary stage combustion rather than lean premixed conditions.

Figure 5 shows the change of a mole fraction of O_2 (%) measured in dry mode with the radial position in the secondary combustor for $T_{VA} = 1673$ K, momentum flux ratio = 5–365 at a pressure of 5 bars. The mole fraction of O_2 was measured from the analysis of the gas samples collected using a movable probe. The radial variation of the mole fraction of O_2 gives valuable information about the radial position of the secondary stage combustion zone in the secondary combustor. The radial position '0' corresponds to the surface of the secondary combustor wall where the methane injector was flush mounted and the position '1' corresponds to the opposite surface as this is the diameter of the secondary combustor. The figure shows that the mole fraction of O_2 exhibits a minimal value at a radial position of 0.3 (i.e., 15 mm) from the wall for the highest value of ΔT (i.e., 169 K), which also corresponds to the highest value of momentum flux ratio (i.e., 365) indicating the possible radial location of the secondary jet flame. The distance between the radial position '0' and the location of the minimal mole fraction of O_2 for each of the profile of the mole fraction of O_2 shown in Fig. 5 is referred to here as penetration depth. The penetration depth varied between 0 and 15 mm for the above-mentioned operating conditions. Hence, the change in momentum flux ratio certainly influenced the penetration depth but not the NO_X formation due to angled injection of methane into vitiated air.

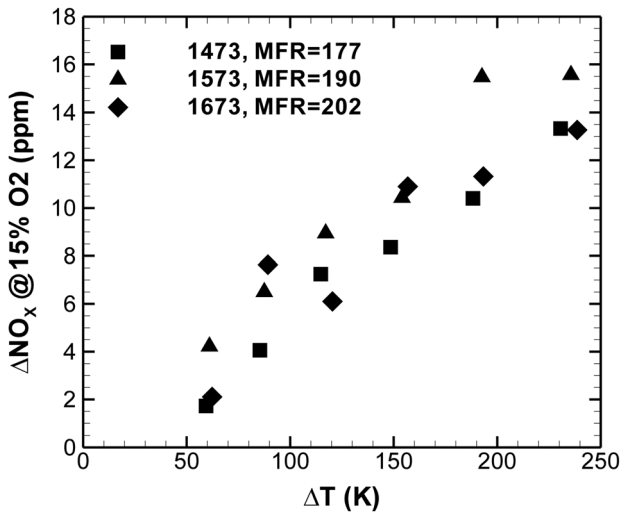

Fig. 6 Mole fraction of ΔNO_x (ppm) at 15% O_2 versus ΔT (K) for different vitiated air temperatures (1473–1673 K) with different momentum flux ratios (177–202) at 5 bars. The first number in the legend title represents the vitiated air temperature (K) and MFR stands for momentum flux ratio.

ΔNO_X Emissions for Constant Momentum Flux Ratio

Figure 6 shows the variation of mole fraction of ΔNO_X corrected to 15% O_2 with ΔT (K) for vitiated air temperatures in the range of 1473–1673 K and momentum flux ratios in the range of 177–202 at a pressure of 5 bars. Different methane injectors with different diameters were used during the experiments to maintain a constant value of momentum flux ratio even with the increasing mass flow rate of methane necessary to increase ΔT. The values of mole fraction of ΔNO_X were obtained by analyzing the samples collected using a static multi port gas probe. The figure shows that the mole fraction of ΔNO_X steadily increased with an increase in ΔT almost in a linear fashion. Another interesting observation is that the mole fraction of ΔNO_X is not affected by the increase in the vitiated air temperature from 1473 K to 1673 K. The reason is that as the temperature of the vitiated air increased, the mole fraction of O_2 simultaneously decreased, and hence the ΔNO_X emissions are independent of change in the vitiated air temperature.

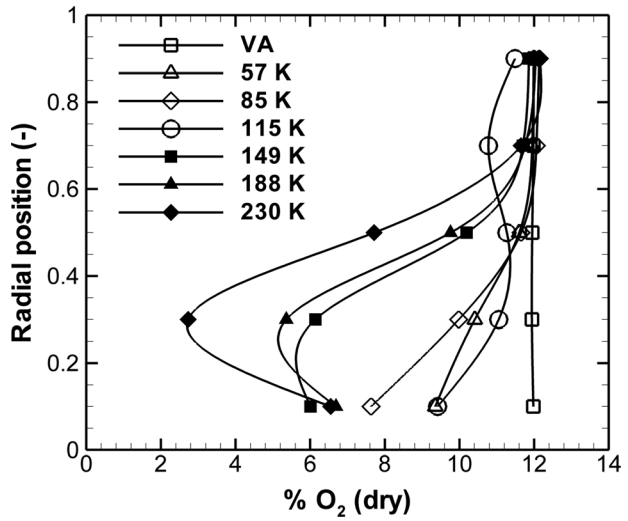

Fig. 7 Mole fraction of O_2 (dry) measured at different radial positions inside the secondary combustor using the movable, single port gas probe for $T_{va} = 1473$ K and momentum flux ratio = 177 at 5 bars. The line legend title represents ΔT in K.

The vitiated air temperature was increased in the following manner during the experiments: (a) mass flow rate of combustion air and its inlet temperature were kept constant, and (b) to increase the vitiated air temperature, the equivalence ratio was gradually increased, leading to a simultaneous decrease in the mole fraction of O_2 in the vitiated air.

Figure 7 shows the variation of mole fraction of O_2 with the radial position inside the secondary combustor for different ΔT (K) for the following operating conditions: $T_{VA} = 1473$ K, momentum flux ratio = 177, and pressure = 5 bars. The local profiles of O_2 inside the secondary combustor were obtained from the analysis of samples collected using a movable single port gas probe. The maximum value of penetration depth obtained for these operating conditions was 15 mm. Foregoing discussions with respect to Figs. 5 and 7 clearly indicate that with the present investigated configuration of angled methane injection into the co-flow direction of a vitiated air cross flow for the investigated momentum flux ratios, the maximum penetration depth obtained was 15 mm.

Numerical Study

Numerical simulation was attempted to study the effect of the secondary injection of methane into vitiated air cross flow. Only the region of interest, the secondary combustor with the methane injection, was chosen as the computational domain and was modeled. The software package ANSYS CFX 11 [18] was used to solve the modeled transport equations for mass, momentum, and scalars, employing the finite volume method approach. The equations were discretized with the high-resolution scheme, which is a second order accurate adaptive blend of the upwind and central difference discretization schemes. The turbulence was modeled using the SST approach [19] with automatic wall functions. The grid refinement near the walls allowed for a mean $y+$ of about 100, with the maximum value below 150.

The grid used in the simulations was mostly composed of hexahedral elements, with a small amount of about 1% of tetrahedral elements on selected regions, in order to improve the grid quality. The grid size is about 1×10^6 nodes. As the vitiated air flows through ceramic foam before entering the secondary combustor, a plug flow velocity profile was applied as a boundary condition. The velocity profile of the methane injection was calculated using an independent CFD simulation of the methane injector, and the resulting velocity field profile was used as boundary condition.

Table 2 Boundary conditions for simulations

Simulation	1	2
Absolute pressure (bar)	5	8
Vitiated air temperature (K)	1673	1673
Mass flow of the vitiated air (kg/h)	279	446
Mass flow of methane (kg/h)	1.603	2.561
Mass composition of the vitiated air		
YO_2	0.0943	0.0911
YCO_2	0.118	0.121
YH_2O	0.0463	0.0474
YN_2	0.7414	0,7405

Two operating conditions, corresponding to the maximum methane injection rate at 5 and 8 bars operating pressure, were simulated. The mass flow of the vitiated air and of the methane injection was scaled with the pressure to develop the same velocity inflow conditions and consequently the same residence time, allowing a direct comparison. The boundary conditions are shown in Table 2.

Turbulent Combustion Modeling. The turbulent reaction modeling of the jet flame anchored in a vitiated air cross flow imposed a significant challenge as it is embedded in a high turbulent flow and burns in a partially premixed mode, two conditions known to cause some reaction models to fail [20]. The applicability of two different reaction models, which differ radically in the modeling of the chemical kinetics and of the turbulence-chemistry interaction, has been investigated. The first approach employed a combination of the eddy dissipation and the finite rate chemistry models to determine the reaction rate, while a presumed joint probability density function (JPDF) model was used in the further investigations.

EDM/FRC

During the implementation of the eddy dissipation and the finite rate chemistry models (EDM/ FRC), the reaction rate is determined as the minimum (process limiting) rate predicted from both models. The details of the implementation can be seen at Ref. [18]. Kheireddine et al. [21] had also used the EDM/FRC model to compute the flame base height of a turbulent methane diffusion flame. The finite rate chemistry was solved using a single step chemical kinetic scheme. Transport equations for all involved major species (CH_4, O_2, CO_2, H_2O, and N_2) have also been solved.

Presumed JPDF. The presumed JPDF model, on the other hand, defines the state of the flow using the mixture fraction f, the reaction progress variable c, and the respective variances f''^2 and c''^2. Transport equations are solved to compute each of the four variables. The reaction rate and the species concentration are read from an adaptive table, containing the results of the detailed chemical mechanism as a function of the four variables described above. More details about the presumed JPDF model can be found in Refs. [22, 23].

The mixture fraction is a conserved passive scalar, and it is defined as

$$f = \frac{(Z_C + Z_H) - (Z_C + Z_H)_{Ox}}{(Z_C + Z_H)_F - (Z_C + Z_H)_{Ox}} \quad (1)$$

where the subscripts O_x and F indicate pure oxidizer and pure fuel, respectively. The mixture fraction of the pure oxidizer has a value of zero, while for the pure fuel it assumes a value of unity. The transport equations for the mean mixture fraction and its variance f''^2 are as follows:

$$\frac{\partial(\overline{\rho}\tilde{f})}{\partial t}+\nabla\left(\overline{\rho}\,\vec{\tilde{u}}\tilde{f}\right)-\nabla\left(\overline{\rho}\left(D+\frac{\nu_t}{Sc_f}\right)\nabla\tilde{f}\right)=0 \tag{2}$$

$$\frac{\partial(\overline{\rho}f''^2)}{\partial t}+\nabla\left(\overline{\rho}\,\vec{\tilde{u}}f''^2\right)-\nabla\left(\overline{\rho}\left(D+\frac{\nu_t}{Sc_{f''^2}}\right)\nabla f''^2\right)$$
$$=C_{f''^2,1}\overline{\rho}\frac{\nu_t}{Sc_{f''^2}}\nabla f''^2\cdot\nabla f''^2-C_{f''^2,2}\overline{\rho}\frac{\tilde{\varepsilon}}{\tilde{k}}f''^2 \tag{3}$$

with $C_{f''^2,1}=2.8$ and $C_{f''^2,2}=2$. Tilde denotes a Favre-averaged quantity.

The reaction progress variable is defined as

$$c=\frac{Z_{O,bounded}-Y_{O_2}}{\min\left(Z_{O,stoich},Z_{O,local}\right)} \tag{4}$$

The progress of the reaction is characterized by c, which assumes a value of zero in the unburned mixture and a value of unity in the totally burned mixture. The reaction progress is a non-passive scalar, and its transport equation includes a reaction source term (Eq. (5)). The same counts for its variance c''^2 (Eq. (6))

$$\frac{\partial(\overline{\rho}\tilde{c})}{\partial t}+\nabla\left(\overline{\rho}\,\vec{\tilde{u}}\tilde{c}\right)-\nabla\left(\overline{\rho}\left(D+\frac{\nu_t}{Sc_c}\right)\nabla\tilde{c}\right)=\overline{\dot{\omega}} \tag{5}$$

$$\frac{\partial(\overline{\rho}c''^2)}{\partial t}+\nabla\left(\overline{\rho}\,\vec{\tilde{u}}c''^2\right)-\nabla\left(\overline{\rho}\left(D+\frac{\nu_t}{Sc_{c''^2}}\right)\nabla c''^2\right)$$
$$=C_{c''^2,1}\overline{\rho}\frac{\nu_t}{Sc_{c''^2}}\nabla c''^2\cdot\nabla c''^2-C_{c''^2,2}\overline{\rho}\frac{\tilde{\varepsilon}}{\tilde{k}}c''^2+2\overline{\dot{\omega}''c''} \tag{6}$$

with $C_{c''^2,1}=2.8$ and $C_{c''^2,2}=2$. The classical gradient diffusion approach is used to close the production and dissipation terms in the transport equations. The clipped Gaussian distribution was used as a presumed shape for the integration process. The chemical reactions system was solved with the GRI-3.0 mechanism [24]. The chosen presumed JPDF method, apart from the chemical kinetics treatment, is similar to current flamelet generated manifolds (FGM) [25] approaches.

Discussion of the Simulation Results. Figures 8 and 9 show the variation of simulated and measured values of mole fraction of O_2 with the radial position of secondary combustor for $T_{VA}=1673$ K at 5 and 8 bars. The radial position was made dimensionless with the combustion chamber diameter. Measurements indicate that the penetration depth of the present configuration changes with combustion chamber pressure. At a pressure of 5 bars, the penetration depth measured was close to a radial position of 0.3, i.e., slightly away from the axis. At a pressure of 8 bars, the measurements indicate that the location of secondary stage jet is very close to the wall. The simulation using the EDM/FRM model was not able to predict this behavior, and the predicted penetration depth remains virtually identical for both 5 bars and 8 bars. The JPDF model, on the other hand, captured the dependence of the penetration depth on the pressure. The reason is that the increase in the pressure affects the chemical kinetics and subsequently the heat release from the flame. Changes in the heat release from the flame affect the temperature field, which in turn influences the evolution of the momentum flux ratio between the methane injection and the vitiated air, leading to a different flame position. A single step chemical kinetic scheme was used with the EDM/FRC model, and hence it could not predict the effects of the increase in the pressure on the chemical kinetics. In this model, the rate of heat release from the flame is influenced mainly by the mixing, and as the mixing is similar for the different pressures, the EDM/FRC model predicts the same flame position for both 5 bars and 8 bars. On the other hand, the JPDF model utilized a detailed chemical kinetic scheme, which causes it to predict the effect of the increase in the pressure on the chemical kinetics and subsequently on the flame position. The qualitative difference in the flame position predicted by both models at 5 bars and 8 bars is displayed in Figs. 8 and 9. The figures assure that the JPDF model is more suitable for the prediction of flame position for the studied operating condition than the EDM/FRC model.

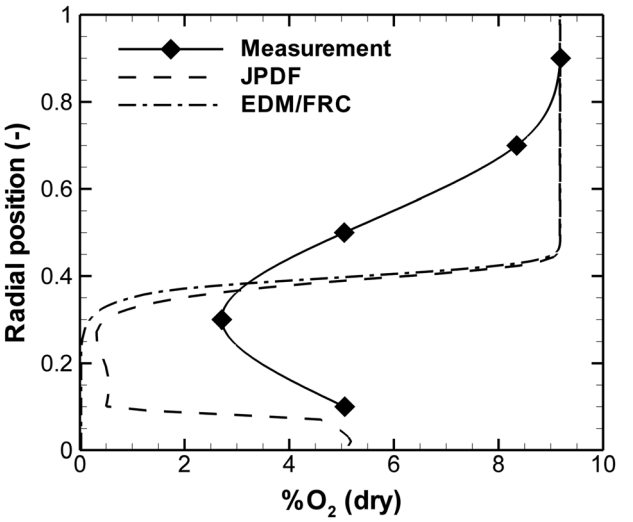

Fig. 8 Comparison of simulated and measured radial profiles of O_2 mole fraction at a pressure of 5 bars. Solid line = measurements, dash-dot line = simulation using EDM/FRC model, anddashed line = simulation using JPDF model.

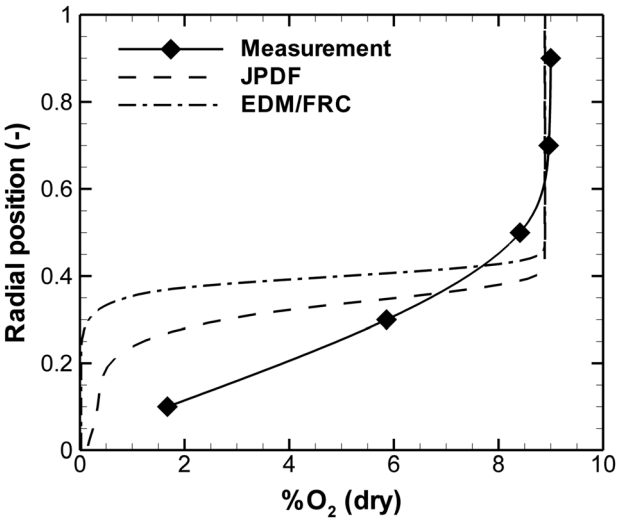

Fig. 9 Comparison of simulated and measured radial profiles of O_2 mole fraction at a pressure of 8 bars. S line = measurements, dash-dot line = simulation using EDM/FRC model, and dashed line = simulation using JPDF model.

A quantitative comparison of the penetration depth of the secondary stage methane jet between the simulations and the measurements is quite difficult for two main reasons: the use of RANS simulation and the uncertainty in the measured vitiated air temperatures. RANS simulations have difficulties in predicting the turbulent mixing in jet and cross flow configurations, which affects the accuracy of the whole simulation [20]. On the other hand, the measured vitiated air temperatures were not corrected for radiation, which corresponds to an uncertainty in the vitiated air velocity, as the mass flow rate was kept constant. The velocity profiles of both jet and cross flow have a significant influence on the

penetration depth, as mentioned in the literature for isothermal systems [20,26]. The investigated system exhibits the same dependency. Further research work is in progress for the better understanding of the influence of a change in the velocity profile of the vitiated air on the penetration depth.

Conclusions

1. For all the investigated operating conditions, the value of a mole fraction of ΔNO_X corrected to 15% O_2 and measured in dry mode was less than 15 ppm.
2. The secondary stage flame was located between 0 mm (i.e., one end of the wall) and 15 mm for the investigated operating conditions at 5 bars, which is slightly away from the axis of the combustion chamber. At higher pressures, it was located closer to the wall where the methane injector was flush mounted.
3. The NO_X formation in the secondary stage was sensitive to the increase in the temperature in the second stage.
4. The NO_X formation was not sensitive regarding the jet velocity, suggesting that quenching phenomena are not of that relevance.
5. The CFD predictions were in closer agreement to the measurements when employing the presumed JPDF model. The non-similarity of the penetration depth with the pressure observed experimentally could be qualitatively predicted by the JPDF model but not by the EDM/FRC model. It is a clear indication that the CFD simulations using the presumed JPDF model are indispensable, as empirical correlations and reaction models based on the similarity of mixing and flow fields will fail to predict this important feature of the system.

Acknowledgment

The present work was financially supported by the Ministry of Research of Baden-Württemberg, Germany together with Siemens AG Germany within the special research initiative "Kraftwerke des 21. Jahrhunderts" ("Power Plants of the 21th Century"). The authors also appreciate the assistance of Mr. Helmut Pabel and Mr. Meinrad Berg for the commissioning of experimental setup.

Nomenclature

T_{VA} = vitiated air temperature
NO_X = nitrogen oxides
ΔNO_X = change in the mole fraction of NO_X with and without secondary stage methane injection
ΔT = change in the adiabatic flame temperature with and without secondary stage methane injection
f = mixture fraction
f''^2 = mixture fraction variance
c = reaction progress variable
c''^2 = reaction progress variable variance
Z_i = element mass fraction of i^{th} species
$\overline{\rho}$ = mean density
D = laminar diffusivity
$\dot{\bar{\omega}}_i$ = reaction rate of i^{th} species
ν_t = turbulent viscosity
u = velocity vector

References

[1] Pitts, W. M., 1988, "Assessment of Theories for the Behavior and Blowout of Lifted Turbulent Jet Diffusion Flames," 22nd International Symposium on Combustion, pp. 809–816.
[2] Peters, N., 2000, *Turbulent Combustion*, Cambridge University Press, Cambridge, UK.
[3] Lyons, K. M., 2007, "Towards an Understanding of the Stabilization Mechanisms of Lifted Turbulent Jet Flames: Experiments," Prog. Energy Combust. Sci., **33**, pp. 211–231.
[4] Lawn, C. J., 2009, "Lifted Flames on Fuel Jets in Co-Flowing Air," Prog. Energy Combust. Sci., **35**, pp. 1–30.
[5] Kalghatgi, G. T., 1981, "Blow-Out Stability of Gaseous Jet Diffusion Flames. Part I: In Still Air," Combust. Sci. Technol., **26**, pp. 233–239.
[6] Kalghatgi, G. T., 1981, "Blow-Out Stability of Gaseous Jet Diffusion Flames Part II: Effect of Cross Wind," Combust. Sci. Technol., **26**, pp. 241–244.
[7] Kalghatgi, G. T., 1982, "Blow-Out Stability of Gaseous Jet Diffusion Flames: Part III - Effect of Burner Orientation to Wind Direction," Combust. Sci. Technol., **28**, pp. 241–245.
[8] Han, D., and Mungal, M. G., 2002, "Stabilization in Turbulent Lifted Deflected-Jet Flames," Proc. Combust. Inst., **29**, pp. 1889–1895.
[9] Johnson, M. R., Littlejohn, D., Nazeer, W. A., Smith, K. O., and Cheng, R. K., 2005, "A Comparison of the Flow Fields and Emissions of High-Swirl Injectors and Low-Swirl Injectors for Lean Premixed Gas Turbines," Proc. Combust. Inst., **30**, pp. 2867–2874.
[10] Littlejohn, D., and Cheng, R. K., 2007, "Fuel Effects on a Low-Swirl Injector for Lean Premixed Gas Turbines," Proc. Combust. Inst., **31**, pp. 3155–3162.
[11] Fokaides, P. A., Kasabov, P., and Zarzalis, N., 2007, "Experimental Investigation of the Stability Mechanism and Emissions of a Lifted Swirl Non-Premixed Flame," ASME Turbo Expo 2007: Power for Land, Sea, and Air, pp. 83–92.
[12] Kasabov, P., and Zarzalis, N., 2009, "Pressure Dependence of the Stability Limits and the NO_X Exhaust Gas Concentrations in Case of Swirl-Stabilized, Diffusion Flames Burning in a Lift-Off Regime," ASME Turbo Expo 2009: Power for Land, Sea, and Air, pp. 613–622.
[13] Cabra, R., Myhrvold, T., Chen, J. Y., Dibble, R. W., Karpetis, A. N., and Barlow, R. S., 2002, "Simultaneous Laser Raman-Rayleigh-LIF Measurements and Numerical Modeling Results of a Lifted Turbulent H_2/N_2 Jet Flame in a Vitiated Coflow," Proc. Combust. Inst., **29**, pp. 1881–1888.
[14] Cabra, R., Chen, J. Y., Dibble, R. W., Karpetis, A. N., and Barlow, R. S., 2005, "Lifted Methane–Air Jet Flames in a Vitiated Coflow," Combust. Flame, **143**, pp. 491–506.
[15] Hayashi, S., and Yamada, H., 2000, "NO_X Emissions in Combustion of Lean Premixed Mixtures Injected Into Hot Burned Gas," Proc. Combust. Inst., **28**, pp. 2443–2449.
[16] Hayashi, S., Yamada, H., and Makida, M., 2005, "Extending Low-NO_X Operating Range of a Lean Premixed–Prevaporized Gas Turbine Combustor by Reaction of Secondary Mixtures Injected Into Primary Stage Burned Gas," Proc. Combust. Inst., **30**, pp. 2903–2911.
[17] Adachi, S., Iwamoto, A., Hayashi, S., Yamada, H., and Kaneko, S., 2007, "Emissions in Combustion of Lean Methane-Air and Biomass-Air Mixtures Supported by Primary Hot Burned Gas in a Multi-Stage Gas Turbine Combustor," Proc. Combust. Inst., **31**, pp. 3131–3138.
[18] ANSYS Europe, Ltd., 2006, ANSYS CFX Release 11.0.
[19] Menter, F. R., 1994, "Two-Equation Eddy-Viscosity Models for Engineering Applications," Am. Inst. Aero. Astro. J., **32**, pp. 1598–1605.
[20] Galeazzo, F. C. C., Donnert, G., Habisreuther, P., Zarzalis, N., Valdes R. J., and Krebs, W., 2011, "Measurement and Simulation of Turbulent Mixing in a Jet in Crossflow," J. Eng. Gas Turbines Power, **133**, pp. 1–10.
[21] Kheireddine, A. S., Chaturvedi, S. K., and Mohieldin T. O., 1999, "Computation of Flame Base Height of a Turbulent Diffusion Flame Resulting From a Methane Jet," JSME Int. J., Ser. B, **42**(1), pp. 78–90.
[22] Wetzel, F., Habisreuther, P., and Zarzalis N., 2006, "Numerical Investigation of Lean Blow Out of a Model Gas Turbine Combustion Chamber Using a Presumed JPDF-Reaction Model by Taking Heat Loss Processes Into Account," Proceedings of ASME Turbo Expo.
[23] Kern, M., Fokaides, P., Habisreuther, P., and Zarzalis, N., 2009, "Applicability of a Flamelet and Presumed JPDF 2-Domain-1-Step-Kinetic Turbulent Reaction Model for the Simulation of a Lifted Swirl Flame," Proceedings of ASME Turbo Expo 2009, Orlando, FL, Paper No. GT2009-5943.
[24] Smith, G. P., Golden, D. M., Frenklach, M., Moriarty, N. W., Eiteneer, B., Goldenberg, M., Bowman, C. T., Hanson, R. K., Song, S., Gardiner, W. C., Jr., Lissianski, V. V., and Qin, Z., "Gri-Mech Home Page," www.me.berkeley.edu/gri_mech/
[25] Vreman, A., Albrecht, B., van Oijen, J., de Goey, L., and Bastiaans, R., 2008, "Premixed and Non-Premixed Generated Manifolds in Large-Eddy Simulation of Sandia Flame D and F," Combust. Flame, **153**, pp. 394–415.
[26] Muppidi, S., and Mahesh, K., 2005, "Study of Trajectories of Jets in Crossflow Using Direct Numerical Simulations," J. Fluid Mech., **530**, pp. 81–100.